Effect of curing temperature on hydration, microstructure and ionic diffusivity of fly ash blended cement paste: A modelling study

Cheng Liu, Mingzhong Zhang*

Department of Civil, Environmental and Geomatic Engineering, University College London, London WC1E 6BT, UK

Abstract: This paper presents an integrated modelling framework to investigate the effect of curing temperature on hydration, microstructure and ionic diffusivity of fly ash blended cement. A 3D cement hydration model, i.e. CEMHYD3D, was modified by incorporating the parameters representing the temperature-dependent dissolution of Portland cement and fly ash and then used to simulate the hydration and microstructural evolution of blended cement with different fly ash replacement ratios and types and water-to-binder ratios cured at various temperatures. Based on the generated 3D microstructure, a lattice Boltzmann model for diffusion was employed to simulate the ionic diffusivity and estimate the relationship between ionic diffusivity and microstructure in hydrating fly ash blended cement paste. Results indicate the simulated hydration process of blended cement cured at various temperatures agrees well with experimental data. The elevated curing temperature leads to a lower capillary porosity and connectivity, less diffusible C-S-H and lower ionic diffusivity at early ages but higher ionic diffusivity later due to the denser hydration products in fly ash blended cement paste.

Keywords: Fly ash; Steam curing; Cement hydration; Pore structure; Diffusivity

1. Introduction

Fly ash (FA) an industrial by-product from the coal combustion, which has been widely utilised to partially substitute cement clinkers for promoting the sustainability of cementitious materials via reducing CO_2 emissions and energy consumption. It was reported that 30% FA substitution for cement clinkers can reduce CO_2 emissions and energy demand by 23% and 21%, respectively [1]. In addition, the proper replacement of cement clinkers with FA can help improve the mechanical performance, transport properties and long-term durability of cementitious materials [2, 3], which can be attributed to the pozzolanic reaction between FA and calcium hydroxide (CH) produced during Portland cement (PC) hydration. As the pozzolanic reaction product, calcium silicate hydrate (C-S-H) further fills the capillary pores and leads to a denser microstructure in comparison with the pure PC-based materials [4]. Meanwhile, due to the reduction of gel porosity [5] and the transformation of chemical composition [6] for C-S-H as a result of the pozzolanic reaction, the intrinsic mechanical and transport properties of pozzolanic C-S-H seem to become better compared to that in pure PC systems [6, 7]. The reaction rates of binders in FA blended cement paste and its microstructural

* Corresponding author. E-mail address: mingzhong.zhang@ucl.ac.uk (M. Zhang)

formation are highly associated with curing temperature [8]. As the rate of pozzolanic reaction is very slow, high-temperature curing, e.g. steam curing [9] and microwave curing [10], is required for high-volume FA concrete to accelerate the reaction of binders and improve the early mechanical properties of concrete. Because of the scientific interest and practical importance, it is vital to gain a comprehensive understanding of the effect of curing temperature on hydration and microstructure of FA blended cement paste.

In the past few decades, some efforts including experimental and modelling studies [11] have been made to explore the effect of curing temperature on hydration and microstructure of FA blended cement paste. Regarding experimental work, Escalante-Garcıa and Sharp [12] measured the hydration degree of PC in FA blended cement paste cured at different temperatures between 10 °C and 60 °C using XRD-Rietveld analysis and reported that FA can slightly promote cement hydration at low curing temperatures but has a detrimental effect at elevated temperatures. Narmluk and Nawa [11] characterised the hydration degree of PC and reaction degree of FA in blended system cured at 20, 35 and 50 °C using XRD-Rietveld analysis and selective dissolution method. They observed that the addition of FA promotes the cement clinker hydration at the temperature lower than 35 °C due to the dilution effect of FA, while the PC hydration is impeded at a higher curing temperature (50 °C) due to the large amounts of pozzolanic C-S-H resulting from the FA pozzolanic reaction at the early age, which counteracts the dilution effect. Weerdt et al. [13] studied the hydration and microstructure of FA blended cement paste cured at various temperatures using image analysis techniques. They found that the rising curing temperature can significantly boost the early reaction degrees of PC and FA, while the pore structure of paste becomes looser in the later period due to the presence of denser C-S-H containing less water and the generation of less high-volumetric ettringite at high temperatures. Although these experimental studies can provide some valuable insights into the reaction mechanisms and microstructure evolution of FA blended cement system at different temperatures, there exists a large discrepancy between the measured data due to the use of different methods [14]. Morevoer, it is still time-consuming to obtain the quantitative information about reaction and microstructure through laboratory experiments considering the variable attributes of local FA for engineering applications.

Modelling is an alternative approach to study the influence of curing temperature on hydration and microstructure of FA blended cement paste. The hydration kinetics of blended cement with various FA mix proportions at different curing temperatures was explored by Wang and Lee [15] and Narmluk and Nawa [11] using the kinetic models based on the shrinking-core theory that was initially applied to PC [16]. Recently, Wang and Ishida [17] proposed a multiphase pozzolanic reaction model by modifying the DuCOM model developed by Maekawa et al. [18] to predict the reaction degree of FA in hydrating binary blended paste considering the effects of curing temperature and FA type. For

FA blended cement paste, the simulated temperature-dependent hydration process agrees well with experimental results. However, the effect of curing temperature on microstructure has not been addressed, which plays a crucial role in deterimining the properties of FA blended cementitious materials. In the past few years, some attempts have been made to simulate the 3D microstructure of FA blended cement paste by incorporating FA pozzolanic reaction into the hydration models of PC. For instance, taking pore solution evolution and CH distribution in blended paste into account, Gao [19] modified the analogical kinetic formulas originally used for PC in the vector-based HYMOSTRUC3D model [20] to simulate the microstructural development of FA binary cement paste. Similarly, Bishnoi et al. [21] introduced the FA pozzolanic reaction by simplifying it as the amorphous silica into μic model [22] for investigating the effect of FA on the microstructural evolution of cement paste. Recently, Liu et al. [23] extended the voxel-based CEMHYD3D model [24] to mimic the hydration and microstructural development of FA blended cement paste by adjusting the initial cellular-automation rules for PC. Nevertheless, to the best of authors' knowledege, the curing temperature-dependent microstructural evolution of FA blended cement paste has not been reflected in any of these models. Thus, it is necessary to develop a suitable hydration model for FA blended cement systems, which can consider the effect of curing temperature on 3D microstructure.

Ionic diffusivity is a critical transport property for evaluating the durability of FA blended cementitious materials and estimating the service life of FA blended concrete structures [25]. The ionic diffusivity of FA blended cementitious materials is highly dependent on the microstructure of cement paste in relation to the curing temperature. The natural diffusion cell test conducted by Cabrera et al. [26] indicated that for the mature FA blended cement paste with a uniform mix ratio, the elevated temperature can lead to an increase in ionic diffusivity as a result of the increasing porosity in the microstructure. Nevertheless, the accurate measurement of ionic diffusivity in cement paste remains a challenge due to the dense microstructure and low penetration of paste, particularly for the FA blended cement system with much denser pore structure. In addition, it is challenging to estimate the effect of each specific influencing parameter on the overall diffusivity of FA blended cement paste from experiments, as their effects are inter-related to each other [27]. To tackle these issues, the authors recently developed a new computational framework for modelling the microstructural development and ionic diffusivity of FA blended cement paste, where the effect of curing temperature has not been considered.

The main purpose of this study is to extend the recently developed computational framework for FA blended cement systems by taking into account the effect of curing temperature on PC hydration and FA pozzolanic reaction, and to estimate the influences of curing temperature, FA content, FA type and water-to-binder (w/b) ratio on microstructure development and ionic diffusivity of cement paste. First, the 3D cement hydration model CEMHYD3D [23] was modified for FA blended cement

system by incorporating the parameters representing the temperature-dependent dissolution of PC and amorphous phases in FA into the model, which were validated with experimental data. Subsequently, the hydration and microstructural development of blended cement paste with different FA contents, FA types and w/b ratios cured at various temperatures were simulated using this modified hydration model. A comparison between the predicted results and the available measured values in terms of reaction degree of FA and hydration degree of PC was carried out for estimating the effect of each variable. Finally, based on the simulated 3D microstructure of FA blended cement pastes cured at various temperatures, a lattice Boltzmann model was employed to simulate the ionic diffusion through the microstructure and investigate the relationship between ionic diffusivity and microstructure in FA blended cement paste in a quantitative manner.

2. Hydration model of blended cement

2.1. Chemical reactions of fly ash blended cement

To simulate the hydration process and microstructural evolution of FA blended cement paste accounting for hydration kinetics, many assumptions and simplifications are required to address such a complex problem in practice [28]. One of the basic simplifications is the use of classic chemical reactions with fixed stoichiometric numbers to represent the thermodynamics of FA blended cement hydration. Therefore, due to lack of thermodynamics information in the simulations, the hydration products obtained from the simulations may deviate from the real ones, in terms of the type of hydration products and stoichiometric numbers. However, this simplification has been widely adopted in the simulations of microstructural evolution and the simulation results of basic hydration indicators agree well with experimental data, especially for Portland cement systems [22, 29]. Hence, the classical chemical reactions [24, 30] were employed to simulate the hydration process and microstructural evolution of FA blended cement paste in this study.

FA blended cement is composed of three components, i.e., cement clinker, gypsum ($C\bar{S}H_2$), and FA, where cement clinker consists of tricalcium silicate (C_3S), dicalcium silicate (C_2S), tricalcium aluminate (C_3A), and tetracalcium aluminoferrite (C_4AF). As PC is mixed with water, C_3S and C_2S react with water to form C-S-H and CH, while C_3A and C_4AF react with water and $C\bar{S}H_2$ leading to the formation of $Fe(OH)_3$ (FH_3), CH, and ettringite ($C_6A\bar{S}_3H_{32}$) or AFm ($C_4A\bar{S}H_{12}$), depending on the content of $C\bar{S}H_2$. Regarding the pozzolanic reactions, FA particles are made up of amorphous and crystalline components, where the amorphous phases normally consist of silicate (S), aluminate-silicate (AS), and calcium-aluminate-silicate (CAS_2) clusters [31, 32]. As illustrated in [24], the amorphous phases in FA particles are composed of S, AS and CAS_2 clusters with fixed stoichiometric numbers, which can react with CH and water to form pozzolanic C-S-H with a lower Ca/Si ratio, stratlingite (C_2AH_8), and FH_3 [24]. The classical chemical reactions of FA blended cement cured at room temperature can be described as follows [24, 30]:

$$C_3S + 5.3H \rightarrow C_{1.7}SH_{3.9} + 1.3CH \quad (1)$$

$$C_2S + 4.3H \rightarrow C_{1.7}SH_{3.9} + 0.3CH \quad (2)$$

$$C_3A + 3C\bar{S}H_2 + 26H \rightarrow C_6A\bar{S}_3H_{32} \quad (3)$$

$$2C_3A + C_6A\bar{S}_3H_{32} + 4H \rightarrow 3C_4A\bar{S}H_{12} \quad (4)$$

$$C_4AF + 2C\bar{S}H_2 + 30H \rightarrow C_6A\bar{S}_3H_{32} + CH + FH_3 \quad (5)$$

$$2C_4AF + C_6A\bar{S}_3H_{32} + 12H \rightarrow 3C_4A\bar{S}H_{12} + 2CH + 2FH_3 \quad (6)$$

$$S + 1.1CH + 2.8H \rightarrow C_{1.1}SH_{3.9} \quad (7)$$

$$AS + 2CH + 6H \rightarrow C_2ASH_8 \quad (8)$$

$$CAS_2 + C_3A + 16H \rightarrow 2C_2ASH_8 \quad (9)$$

$$CAS_2 + C_4AF + 20H \rightarrow 2C_2ASH_8 + CH + FH_3 \quad (10)$$

2.2. Modelling of temperature-dependent hydration of blended cement

In our previous study [23], the voxel-based CEMHYD3D hydration model has been modified to mimic the hydration and microstructure of FA blended cement paste cured at room temperature. The entire modelling procedure can be briefly described as follows. First, according to the w/b ratio, binder powder size, and FA replacement level, the packing of blended cement was established by randomly throwing binder particles into a cubic representative volume element (RVE) from the large particles to the small ones. For the blended cement system, the size of the cubic system was set as 200 × 200 × 200 μm^3 with a default resolution of 1 μm/voxel. Afterwards, based on the content and distribution of mineral phases in binders (PC and FA), the voxels of cement clinkers in the generated packing were segmented into C_3S, C_2S, C_3A and C_4AF, while those of FA were divided into reactive phases (S, AS, and CAS_2) and inert phases (mullite, quartz, etc.). Finally, the computational cycles consisting of dissolution, diffusion and reaction iteration manipulated by the cellular automaton-based evolution rules along with various empirical dissolution and reaction probabilities were employed to simulate the aforementioned chemical reactions of FA blended cement, i.e. Eqs. (1)-(10), and 3D microstructural development. Using a conversion factor (β) that is mainly dependent on the resolution in the modified CEMHYD3D, the real-time (t) can be correlated with computational cycles (n) as:

$$t = \beta n^2 \quad (11)$$

The change of curing temperature has a twofold effect on the hydration and microstructure of FA blended cement. The higher curing temperature can promote the reaction rates of binders, while the precipitating hydration products at higher temperatures are heterogeneously distributed, leading to denser C-S-H gels and coarser capillary pores. In the modified CEMHYD3D model, the influences of curing temperature on the rates of PC hydration and FA pozzolanic reaction were respectively reflected by introducing a temperature-dependent conversion factor (see Eq. (11)) and dissolution probability of FA. Note that although the dissolution probabilities of mineral phases in PC are kept

constant in the simulations, the conversion factor extended as a function of curing temperature can equivalently describe the temperature-dependent dissolution probability of PC [30]. The relationship between conversion factor (β) and curing temperature (T) can be expressed as:

$$\beta = \beta_{298}/k_C \tag{12}$$

$$k_C = exp\left[-\frac{1000E_C}{R}\left(\frac{1}{T+273}-\frac{1}{298}\right)\right] \tag{13}$$

where k_C is a factor based on the Arrhenius equation, β_{298} is the basic conversion factor at 25 °C, normally set as 0.00035 h/cycle[2] for the resolution of 1 μm/voxel [30, 33], E_C is the PC activation energy (40 kJ/mol [30]), and R is the gas constant.

The dissolution probabilities of amorphous phases in FA affected by the curing temperature can be described as:

$$P_{FAi} = P_i^0 \frac{k_{FA}}{k_C} \tag{14}$$

$$k_{FA} = exp\left[-\frac{1000E_{FA}}{R}\left(\frac{1}{T+273}-\frac{1}{298}\right)\right] \tag{15}$$

where P_{FAi} denotes the dissolution probability of amorphous phase i, P_i^0 the pre-defined basic dissolution probability of amorphous phase i at 25 °C, k_{FA} is a factor determined using the Arrhenius equation, and E_{FA} is the FA activation energy that is 80 kJ/mol [30].

To simulate the denser hydration products in blended cement paste cured at a higher temperature, the intrinsic C-S-H porosity and C-S-H distribution in microstructure were respectively expressed to be temperature-dependent. In FA blended cement paste, it is assumed that there exist two kinds of C-S-H gels, i.e. $C_{1.7}SH_{3.9}$ from PC hydration and $C_{1.1}SH_{3.9}$ from pozzolanic reaction. For the C-S-H from PC hydration ($C_{1.7}SH_{3.9}$), its stoichiometry can be expressed as a function of temperature, at which the reactions occur [30]:

$$V_{CSH} = \begin{cases} V_{CSH}^0 - 8 \times \frac{T-20}{80-20} & T < 80\ °C \\ V_{CSH}^0 - 8 & T \geq 80\ °C \end{cases} \tag{16}$$

$$n_w = \begin{cases} n_w^0 - 1.3 \times \frac{T-20}{80-20} & T < 80\ °C \\ n_w^0 - 1.3 & T \geq 80\ °C \end{cases} \tag{17}$$

where V_{C-S-H} represents the molar volume of C-S-H, V_{C-S-H}^0 stands for the basic molar volume of C-S-H at 20 °C that is equal to 108 cm^3/mol, n_w denotes the H/S ratio in C-S-H, and n_w^0 is the basic H/S ratio in C-S-H at 20 °C that is equal to 3.9.

Regarding the C-S-H from the pozzolanic reaction ($C_{1.1}SH_{3.9}$), the molar volume and stoichiometry are considered to be not temperature-dependent as the intrinsic gel porosity of pozzolanic C-S-H with 0.19 [5] is much lower than that of C-S-H from PC with 0.28 [34] at 20 °C [7]. For the C-S-H gels, they are normally regarded as a fractional structure composed of a larger number of basic spherical building blocks with a diameter of 2.2 nm [35]. As the volume of the basic

building block is not affected by curing temperature [36], the intrinsic gel porosity of C-S-H produced from PC (ϕ_{CSH}) related to curing temperature can be expressed as:

$$\phi_{CSH} = 1 - \frac{0.72V_{CSH}^{0}}{V_{CSH}} \quad (18)$$

Regarding the C-S-H distribution in microstructure, a temperature-dependent cubic box is introduced, which can affect the distance of dissolved C-S-H voxels from the dissolution surface of cement particles. When the voxel of C_3S or C_2S is determined for dissolution, this dissolved voxel is removed and a dissolved C-S-H voxel is generated at a capillary pore voxel beside this dissolution point. Meanwhile, to keep the correct volume stoichiometry of the chemical reactions, an extra dissolved C-S-H voxel is statistically created and placed at a random capillary pore voxel near this dissolution point within a $2b \times 2b \times 2b$ cubic box centred at the dissolution point. The dissolved C-S-H voxels can randomly walk in the effective pores until precipitating on the solid surface. A denser C-S-H layer formed around the unhydrated cement can be achieved by decreasing *b*, which results in the coarser capillary pores and a decrease in the ultimate reaction degree of cement at the later curing ages. The value of *b* as a function curing temperature can be expressed as:

$$b = Max\left[1, int\left\{3 + 5 \times \frac{40-T}{20}\right\}\right] \quad (19)$$

where *Max* and *int* denote the maximum and integer functions, respectively.

2.3. Determination of input parameters

To determine the pre-defined input parameters, e.g. dissolution probabilities of mineral phases in PC and amorphous phases in FA, the simulated hydration process was compared with the experimental data. Here, the reaction degree of FA in binary cement paste measured using the selective dissolution method was employed to calibrate the pre-defined parameters. The PC employed is a Chinese standard cement named P.I. 52.5, the Blain fineness and density of which are 369 m^2/kg and 3.15 g/cm^3, respectively. The mass fractions of mineral phases are 56.00% C_3S, 25.66% C_2S, 7.49% C_3A, and 10.85% C_4AF (see Table 1). A low-calcium FA with the Blain fineness of 469 m^2/kg and density of 2.24 g/cm^3 was utilised, which is composed of 64.59% amorphous phase and 35.41% inert phase, including 11.77% mullite and 23.64% quartz. To determine the content of specific amorphous phases, the following assumptions were made for the FA clusters: (1) The CAS_2 completely takes up the CaO in the amorphous phases. (2) The amorphous Al_2O_3 prefers to exist in the CAS_2, while the remaining Al_2O_3 constitutes the amorphous AS. (3) Except for the SiO_2 in CAS_2 and AS, the residual amorphous SiO_2 directly forms the silicate cluster. As shown in Table 2, the obtained volume fractions of phases in FA are 19.3% CAS_2, 20.9% AS, 22.4% S, and 37.4% inert phase.

In the simulation, the pre-defined dissolution probabilities of mineral phases in PC in the binary system were kept unchanged since the simulated results using these parameters can give a good estimation of the hydration and pore structure of the pure PC system [30]. A comparison between the

simulated and experimental reaction degree of FA in the blended paste with w/b = 0.50 and FA contents of 10%, 30% and 50% (see Fig. 1) indicates that the basic dissolution probabilities for amorphous phase clusters can be all treated to be 0.08, i.e. $P_i^0 = 0.08$ in Eq. (14). Here, it is worth noting that the reaction degree of FA in the blended cement paste was measured using the selective dissolution method as per the Chinese standard GB/T 12960-2007. More details about this can be found in a previous publication [23]. Although the dissolution rates of amorphous phases with different chemical compositions in FA would vary in reality [32], which can be also implemented in the simulation. However, it is far from trivial to accurately characterise the reaction rates of different amorphous phases through experiments. Meanwhile, the other simulated indicators of hydration process for FA blended paste, e.g. hydration heat and CH content, also agree well with experimental data when using the same basic dissolution probability for all amorphous phases [23]. Therefore, the dissolution rates of amorphous phases with different chemical compositions in FA are assumed to be identical in the simulation. Taking the blended cement paste with w/b = 0.50 and FA content of 30% as an example, Fig. 2 displays the simulated volume fractions of solid phases and capillary pore cured at 20 °C against curing age. It can be found that the PC hydration mainly occurs within the first few days, while the FA pozzolanic reaction is not significant but can last for a long period, which is confirmed by the increasing content of C_2ASH_8 and C-S-H during the entire reaction process.

3. Effect of curing temperature on hydration process

Based on the pre-defined parameters determined in Section 2.3, the curing temperature-dependent hydration process of FA blended cement paste can be simulated. Here, the specific raw materials studied in [13, 17, 37] in terms of mineral phases and fineness of binders (see Table 1) were selected for simulation and the emphasis was placed on the influences of FA content, FA type, and w/b ratio on hydration process of cement paste at various curing temperatures. According to the chemical information and crystal phases of FA provided in [13, 17, 37] (see Table 1), the volume fractions of various amorphous phases and inert phase in the simulation were calculated and presented in Table 2. A comparison between the simulation results and experimental data adopted from literature [13, 17, 37] was carried out for validation.

3.1. Blended cement paste with different fly ash contents

The effect of FA content on the reaction degree of FA and hydration degree of PC in blended cement paste cured at different temperatures was investigated by Weerdt et al. [13] using image analysis techniques. In their study, the used PC is composed of 58.70% C_3S, 20.65% C_2S, 11.95% C_3A, and 8.70% C_4AF by mass and has a Blain fineness and density of 450 m^2/kg and 3.15 g/cm^3, respectively. A class F siliceous FA was utilised, the chemical composition and physical properties of which are presented in Table 1. According to the XRD-Rietveld analysis, FA consists of 64.59% amorphous phase, 11.77% mullite and 23.64% quartz by mass. The Blain fineness and density of FA are 450

m^2/kg and 2.74 g/cm^3, respectively. The volume fractions of different amorphous phases as inputs in the simulation are 36.06% CAS_2, 1.43% AS, 30.09% S, and 32.42% inert phase. The blended cement paste specimens with w/b = 0.50 and FA contents of 30% and 35% were prepared and cured in CH saturated solution at 5, 20 and 40 °C until the ages for testing.

Fig. 3 shows the simulated and measured results of reaction degree of FA and hydration degree of PC in the FA blended cement system. It can be seen that the reaction degree of FA and hydration degree of PC both increase with the increasing curing age but exhibit different rising trends. The reaction degree of FA continuously increases during the entire reaction process, while the hydration degree of PC is mainly increased in the early period, i.e. within 10 d. Moreover, for all blended cement pastes, the ultimate hydration degree of PC is much higher than the reaction degree of FA. For instance, the ultimate hydration degree of PC and reaction degree of FA in blended cement paste at 200 d are around 90% and less than 35%, respectively. The difference in changing trend and ultimate reaction degree between FA and cement can be attributed to the discrepancy of their chemical reactivity [38]. Regarding the effect of curing temperature, for the blended cement paste with the same FA content, the elevated curing temperature can promote the reaction of FA during the entire reaction process, which leads to a higher ultimate reaction degree of FA. For instance, as the curing temperature increases from 5 °C to 40 °C, the relation degree of FA is doubled to 35% after 200 d of curing. Nevertheless, the PC hydration is only significantly accelerated by the elevated curing temperature within the first few days. The hydration degree of PC at a low curing temperature can approach or even surpass that at a higher curing temperature, also indicated in Fig. 4b. This can be explained by the fact that the denser hydration products produced at elevated temperatures around unhydrated cement particles are detrimental to the further cement hydration in the later period [39], which offsets the contribution resulting from the increasing temperature. Regarding the effect of FA content, for the blended cement paste cured at the same temperature, the higher FA content is beneficial to the increase in hydration degree of PC due to the increasing dilute and nucleation effects [40]. However, the pozzolanic reaction is retarded for a higher FA content because of the weaker activated ability of pore solution for FA as a result of lower pH and Ca^{2+} concentration [4]. Additionally, the difference of reaction degree of FA between 30% and 35% replacement ratios becomes more significant when the cement paste is cured at a higher curing temperature, e.g. 40 °C. In comparison with the experimental data obtained by Weerdt et al. [13], the simulated reaction degree of FA at later curing ages and hydration degree of PC at early curing ages are smaller. The difference can be attributed to the following aspects: (i) during the image processing, the filtration would lead to the loss of the superfine binders including PC and fly ash particles and thus result in an overestimation of the reaction degree at early curing ages [41]; (ii) some assumptions and simplifications were made for the cement hydration models. For instance, the potential influences of

chemistry and synthesis conditions on reaction of FA in the system were ignored, which would inevitably lead to the discrepancy as compared with experimental data. In general, there exhibits an acceptable level of agreement between simulations and experiments in terms of the coupled effect of FA content and curing temperature.

3.2. Blended cement paste with different fly ash types

Fig. 4 shows the effect of FA type on temperature-dependent hydration process of blended cement system with w/b = 0.40 and FA content of 30%, in terms of reaction degree of FA and hydration degree of PC, where the experimental results obtained by Wang and Ishida [17, 42] using the selective dissolution method and XRD-Rietveld analysis were selected for comparison. Two types of FA (FA I and FA II) and two curing temperatures (20 and 60 °C) were considered for simulation. In the simulation, all inputs were kept identical to those used in experiments. In detail: the PC used is composed of 65.50% C_3S, 15.90% C_2S, 8.07% C_3A, and 8.77% C_4AF by mass, the Blain fineness and density of which are 335 m^2/kg and 3.15 g/cm^3, respectively. Two types of low-calcium FA (FA I and FA II) with a similar fineness (around 400 m^2/kg) were employed, the detailed information of which regarding chemical composition and physical properties are summarised in Table 1. The calculated volume fractions of FA I and FA II are presented in Table 2.

As seen in Fig. 4, the simulated and experimental hydration process both indicate that the chemical composition and mineral phase of FA significantly influence the FA pozzolanic reaction. For instance, in the FA blended cement paste cured at 60 °C for 182 d, the reaction degree of FA II (17.5%) is only 78% that of FA I (22.5%). This finding is expected because the reaction activity of FA is increased with the increasing content of amorphous phase [43], which leads to a higher reaction degree of FA I compared to FA II. However, as shown in Fig. 4b, the PC hydration in the blended paste is not obviously affected by the FA type, which is identical to the findings by Sofi et al. [44], who reported that the FA with different chemical compositions but similar fineness displays a slight influence on the measured hydration degree of PC. The comparison between simulations and experiments indicates that there exists an obvious difference in the simulated and experimental results of reaction degree of FA II at 20 °C in the early period. Apart from the limitations of the hydration models, it can be explained by the fact that the selective dissolution method used in [17, 42] may lead to the underestimation of the reaction degree of fly ash due to the incomplete dissolution of cement and hydration products [41]. However, the simulations and experiments are in good agreement in terms of changing trend and the reaction degree of FA and hydration degree of PC for the other blended cement paste specimens. It suggests that the modified CEMHYD3D model can provide a good estimation of the temperature-dependent hydration of blended cement paste with different types of FA.

3.3. Blended cement paste with different w/b ratios

Fig. 5 displays the predicted reaction degree of FA in blended cement pastes with various w/b ratios (0.30 and 0.50) and FA content of 40% at curing temperatures of 20 and 40 °C as a function of curing age along with the corresponding experimental data acquired by Hanehara et al. [37] using the selective dissolution method. From this figure, the coupled effect of w/b ratio and curing temperature on the hydration process of FA blended cement system can be estimated. In their experiments, PC with a density of 3.13 g/cm^3 and Blaine fineness of 337 m^2/kg, and low-calcium FA with a density of 2.33 g/cm^3 and Blaine fineness of 400 m^2/kg were used to prepare the specimens. The well-mixed FA blended specimens with w/b = 0.30 and 0.50 and FA content of 40% were cured in plastic vessels at 20 and 40 °C, respectively. Since the information about chemical compositions and mineral phases in PC and FA were not provided in [37], the PC used in Wang and Ishida [17] was adopted in the simulation because of the similar fineness and the same country of manufacture. Regarding FA, the volume fractions of mineral phases used in [23] were employed in the simulation here considering the similar chemical compositions of FA studied.

It can be found from Fig. 5 that for the blended pastes cured at the same age, the increasing w/b ratio can lead to a higher reaction degree of FA. For instance, when w/b ratio increases from 0.30 to 0.50, the reaction degree of FA in the paste cured at 20 °C for 365 d is increased by 43% from 17.4% to 25.6%. Such increase can be ascribed to the fact that for the blended paste with a higher w/b ratio the more water for the reaction and more space for the reaction products to form are available in the microstructure [2]. For the blended paste cured at 20 °C, the simulated reaction degree of FA before 100 d of curing seems to be higher than the experimental data, which can be attributed to the discrepancy of mineral phases in raw materials. However, for the remaining FA blended cement pastes cured at 40 °C or in the later period, the simulated results are in good agreement with the experimental data, which suggests that the effect of w/b ratio on temperature-dependent hydration process of FA blended cement paste can be predicted with acceptable accuracy using this modified CEMHYD3D model.

4. Effect of curing temperature on microstructural evolution

After the validation of the modified CEMHYD3D model with experiments in terms of hydration process, the model was used to simulate the microstructural evolution of FA blended cement paste at different curing temperatures. Here, the raw materials and mix proportions used in the experiments carried out by Wang and Ishida [17] were selected and incorporated into the model for simulating the temperature-dependent microstructure development of FA blended cement paste as different types of FA can be considered. Figs. 6 and 7 show the evolution of solid phases and capillary pores in the paste microstructure with w/b = 0.40 and FA I content of 30% cured at 20 and 60 °C, respectively. As seen in Fig. 6, with the increasing curing age, the binders reactions with water gradually occur, the hydration products of which bring about a reduction in the capillary pore space. Moreover, the

rate of FA pozzolanic reaction is far slower than the PC hydration rate. For example, compared to the vague outline of PC particles after 28 d of curing, the intact large FA particles can be clearly differentiated from the hydrating blended paste cured after 180 d. This finding is confirmed by Durdziński et al. [45] who demonstrated that for the binary blended cement paste cured after 90 d, the experimental pozzolanic degree of FA is still less than 30%. In terms of the influence of curing temperature on the paste microstructure, it can be found that the elevated curing temperature from 20 °C to 60 °C promotes the PC hydration and surface erosion of FA particles before 3 d of curing. After 28 d of curing, the hydration degree of PC cured at 20 °C is close to that cured at 60 °C, but the erosion degree of FA particle in paste cured at 60 °C is still more significant compared to the paste cured at 20 °C. These findings are consistent with those of the hydration process indicated in Fig. 4. The evolution of capillary pores including connected and unconnected pores against curing age is plotted in Fig. 7. The decreasing capillary porosity due to the expanding hydration products results in a more tortuous capillary pore structure and brings about the decreasing connectivity of capillary pore determined using the burning algorithm [46]. Furthermore, the evolution of capillary pores in FA blended cement paste is also correlated with the curing temperature. It can be observed that the increasing curing temperature before 28 d of curing is beneficial to the decrease in the connectivity of capillary pore due to the promotion of reactions of PC and FA. Nevertheless, after 28 d of curing, the elevated curing temperature is detrimental to the decreasing volume fraction of connected capillary pore, which can be ascribed to the higher overall reaction degree of FA blended cement and the denser hydration products that will be discussed later.

To quantify the effect of curing temperature on capillary pore structure, the evolution of capillary porosity and connectivity of capillary pore is indicated and discussed in detail. Fig. 8 shows the capillary porosity with curing age in blended pastes with FA I and FA II cured at 20, 40, and 60 °C. It can be observed that for the blended cement paste cured at the same age, the increasing curing temperature can lead to a lower capillary porosity in the early period for both FA I and FA II. However, the capillary porosity of cement paste cured at a lower temperature gradually tends to be close to and finally lower than that cured at a higher temperature in the later period. This simulated changing trend is similar to the experimental findings by Escalante-Garcıa and Sharp [39] based on the analysis of backscattered scanning images of FA blended cement paste after 1-year curing that the porosity of paste cured at 60 °C is higher than that cured at 10 °C. In addition, it can be found that the evolution of capillary porosity is also dependent on the FA type. Compared to the FA II with lower chemical reactivity, the capillary porosity of blended cement paste with more reactive FA I is consistently lower, when the curing temperature is kept the same. This is expected as the chemical composition and mineral phase in FA are crucial to the hydration process of blended cement paste [8], and the FA pozzolanic reaction with higher reactive activity is more sensitive to the elevated curing temperature

(see Fig. 4a). The overall reaction degree of FA blended cement (PC and FA) against curing age is also displayed in Fig. 8. It can be seen that with the increase of curing age, the increasing overall reaction degree is consistent with the decreasing capillary porosity for all cement pastes. This implies that the effect of curing temperature on capillary porosity in microstructure can be ascribed to the change of overall reaction degree of binders as a result of curing temperature change.

Fig. 9a shows the evolution of connectivity of capillary pore with curing age in FA blended cement paste with w/b = 0.40 and FA content of 30% at 20, 40 and 60 °C. It is indicated that there exists a similar decreasing trend between the connectivity and volume fraction of capillary pore in cement paste against curing age, while the lower capillary porosity does not strictly correspond to the lower connectivity of capillary pore for blended cement pastes cured at different temperatures. The relationship between connectivity of capillary pore and capillary porosity in FA blended cement paste is depicted in Fig. 9b. It can be observed that for the cement paste with the same capillary porosity prior to capillary depercolation, the elevated curing temperature results in larger connectivity of capillary pore, which can be ascribed to the coarser pore size as a result of the increasing curing temperature. This can be confirmed by the 3D connected capillary pores of FA blended cement paste cured at 20 and 60 °C with a porosity of 0.23 shown in Fig. 9b. It suggests that the modifications mentioned in Section 2.2 for simulating the coarser pores in microstructure cured at a higher temperature are effective. As the capillary porosity approaches the depercolation threshold, the elevated curing temperature yet results in lower connectivity of capillary porosity in FA blended cement paste. Moreover, with the increase of curing temperature, the depercolation threshold of capillary porosity is decreased. These changing trends of connectivity of capillary pore related to capillary pore size are similar to those of connectivity of inclusion with inclusion size in a two-phase composite medium presented in [47]. A comparison between the results for FA I and FA II indicates that the FA type has an obvious influence on the development of capillary porosity with curing age (see Fig. 8), while the relationship between connectivity of capillary pore and capillary porosity is not significantly changed when the curing temperature is kept the same (see Fig. 9b). This can be explained by the fact that the distribution of reaction products in the microstructure of blended cement paste is not affected by the FA type.

5. Effect of curing temperature on ionic diffusivity

According to the generated 3D paste microstructure cured at various temperatures, a lattice Boltzmann model [48] was employed to mimic the ionic diffusion through the paste microstructure and estimate the ionic diffusivity of cement paste. First, the voxel-based microstructure simulated using the modified CEMHYD3D model was converted into a four-phase composite medium comprised of capillary pores, two C-S-H gels respectively produced from the PC hydration and FA pozzolanic reaction, and non-diffusive solid phases including unreacted binders (cement and FA) and

other hydration products. After that, the ionic diffusivities of pore water in capillary pores and C-S-H as inputs need to be determined for the lattice Boltzmann simulation. For the pore water of capillary pore, its ionic diffusivity (D_0) is set as 2.03×10^{-9} m^2/s [49], while the ionic diffusivity of C-S-H (D_{CSH}) can be expressed using the following equation [50]:

$$D_{CSH} = D_{GP}[0.059\phi_{CSH} + 0.226(\phi_{CSH})^{3.68}] \quad (20)$$

where ϕ_{CSH} denotes the C-S-H porosity, and D_{GP} is the ionic diffusivity of pore water in gel pore, normally set as 10^{-10} m^2/s [51], which is lower than D_0 because of the incremental viscosity of pore water [51] and electrical double layer effect [52] in gel pore with nanometers.

As mentioned in Section 2.2, it is assumed that there exist two kinds of C-S-H gel in FA blended cement paste. The gel porosity of C-S-H produced from PC hydration is temperature-dependent, following Eqs. (16) and (18), while the gel porosity of pozzolanic C-S-H produced from FA pozzolanic reaction is not affected by the curing temperature that is equal to 0.19. Accordingly, the ionic diffusivities of C-S-H produced from PC hydration at curing temperatures of 20, 40 and 60 °C can be calculated as 1.86×10^{-12} m^2/s, 1.71×10^{-12} m^2/s and 1.55×10^{-12} m^2/s, and the ionic diffusivity of pozzolanic C-S-H is 1.17×10^{-12} m^2/s. Afterwards, the lattice Boltzmann simulation was applied to the FA blended cement paste for simulating the ionic diffusion. The modelling procedure including the collision step and streaming step was iterated until the steady-state diffusion was reached. As the ionic concentration distribution under the steady-state in cement paste is acquired, its ionic diffusivity can be quantified according to Fick's first law. Taking the FA blended cement paste with w/b = 0.4 and FA content of 30% as an example, the simulated steady-state ionic diffusion in the paste microstructure cured at 20 °C and 60 °C for 28 d is shown in Fig. 10. It is indicated that the ionic distribution in blended cement paste is non-uniform due to the heterogeneously distributed diffusible phases in the microstructure.

Fig. 11a displays the ionic diffusivity versus curing age in FA blended cement paste cured at 20, 40 and 60 °C. It can be observed that with the increase of curing age, the ionic diffusivity is decreased in blended paste, which can be mainly attributed to the decreasing fraction and connectivity of capillary pore as a result of the continuous chemical reaction. For the FA blended cement paste with the same replacement level, the elevated temperature can bring about a lower ionic diffusivity in the early period but a higher one in the later period, which agrees well with the experimental findings indicated by Ramezanianpour and Malhotra [53]. In their experiments, the resistance of FA blended cement concrete cured at 38 °C to chloride penetration is better than that cured at a standard curing temperature before 28 d of curing but the result is opposite after that. For the cement paste, its ionic diffusivity is directly associated with the capillary porosity and connectivity of capillary pore in the microstructure [54]. As can be seen, the change of ionic diffusivity with curing age shows a similar trend with that of capillary porosity against curing age discussed in Section 4. In addition, the elevated

curing temperature results in higher connectivity of capillary pore due to the coarser pore structure and the ionic diffusivity is accordingly increased for the blended cement paste cured at a higher temperature. Fig. 11b shows the ionic diffusivity as a function of capillary porosity in blended cement paste, which indicates that the elevated curing temperature is detrimental to the decrease of ionic diffusivity. The ionic diffusivity of blended cement paste with different FA types can also be seen in Fig. 11b that the FA with higher reactive activity (FA I) results in a lower ionic diffusivity. This is expected because the FA with higher reactivity can promote the pozzolanic reaction, leading to a smaller capillary porosity (see Fig. 8).

Fig. 12 shows the ionic diffusivity against accessible capillary porosity in FA blended cement paste cured at various temperatures. It can be observed that for the cement paste with accessible capillary porosity larger than 0 (prior to the capillary depercolation), the logarithmic ionic diffusivity linearly increases with the accessible capillary porosity, regardless of curing temperature and FA type. After the accessible capillary porosity is equal to 0 (i.e. capillary depercolation), the ionic diffusivity decreases slightly with the decrease of capillary porosity (see Fig. 11b), which can be attributed to the smaller diffusivity of diffusible C-S-H gels that act as the dominant diffusion paths. Despite not being shown here, it can be expected that the less diffusable C-S-H gels in blended cement paste cured at a higher temperature are likely to be beneficial to the decrease in its ionic diffusivity after the capillary depercolation is reached [7]. This finding can be confirmed by the decreasing ionic diffusivity with the elevated curing temperature for the FA blended cementitious materials with a lower w/b ratio or cured in the later period. For instance, Li et al. [55] demonstrated that the measured ionic diffusivity of FA blended concrete with a lower w/b ratio (0.35) decreases with the increase of curing temperature between 10 °C and 40 °C in the later period.

6. Conclusions

In this study, an integrated modelling framework was developed to investigate the influence of curing temperature on hydration process, microstructural evolution and ionic diffusivity of fly ash blended cement system. CEMHYD3D model was further modified to mimic the temperature-dependent hydration and microstructural development of blended cement system with different fly ash contents (between 10% and 50%), fly ash types and water-to-binder ratios (ranging from 0.30 to 0.50). According to the simulated 3D microstructure, a lattice Boltzmann model was employed to estimate the ionic diffusivity of blended paste cured at different temperatures (20, 40 and 60 °C), which provides comprehensive insights into the relationship between ionic diffusivity and paste microstructure cured at various temperatures. The main conclusions can be drawn as follows:

- The Arrhenius law and temperature-dependent pore size were successfully introduced into the CEMHYD3D model for simulating the influence of curing temperature on hydration and microstructure of fly ash blended cement system. The simulated temperature-dependent hydration

process of blended cement system with different fly ash contents, fly ash types, and water-to-binder ratios agrees well with experimental data obtained from the literature.

- The elevated curing temperature can accelerate the pozzolanic reaction of fly ash during the entire reaction process, while the Portland cement hydration is only promoted within the first few days. The hydration degree of Portland cement at a lower curing temperature can surpass that at a higher curing temperature in the later period, which can be ascribed to the denser C-S-H gels produced at elevated temperatures around unhydrated cement particles, leading to a detrimental effect on the further hydration of Portland cement.
- The elevated curing temperature contributes to the decrease in the connectivity of capillary pore at the early curing ages (before 28 d) because of the promotion of reactions of Portland cement and fly ash. Nevertheless, in the later period (after 28 d), the higher curing temperature has a detrimental effect on the decreasing volume fraction of connected capillary pores as a result of the lower overall reaction degree of fly ash blended cement and the denser C-S-H gels.
- Owing to the decreasing capillary porosity as a result of the promotion of binder reactions and the higher connectivity of capillary pore resulting from the coarser pore structure, the increase of curing temperature can lead to a lower ionic diffusivity of blended cement paste in the early period but a higher one in the later period. Before the capillary depercolation, a unique linear increase of the logarithmic diffusivity with the accessible capillary porosity can be observed, regardless of curing temperature and fly ash type. The less diffusable C-S-H gels in fly ash blended cement paste cured at a higher temperature are beneficial to the decrease of its ionic diffusivity after the capillary depercolation is reached.

Although this model can well estimate the hydration, microstructure and transport property of fly ash blended system cured at various temperatures, the following aspects still need to be further addressed: (1) In the present model, the decomposition of solid phases cured at an elevated temperature (over 60 °C), e.g. decomposition of ettringite [56], is ignored. (2) The real phase assemblage of temperature-dependent hydration products of fly ash blended system needs to be considered, possibly in combination with thermodynamic modelling [57]. (3) The relationship between the ionic diffusivity in C-S-H and its composite can be investigated in a quantitative manner [58].

Acknowledgements

The authors gratefully acknowledge the financial support from the Engineering and Physical Sciences Research Council (EPSRC), UK under Grant No. EP/R041504/1 and the Royal Society, UK under Award No. IEC\NSFC\191417 as well as the Visiting Researcher Fund Program of State Key Laboratory of Water Resources and Hydropower Engineering Science, China under Award No. 2019SGG01. The financial support provided by University College London (UCL) and China

Scholarship Council (CSC) to the first author is also gratefully acknowledged.

References

[1] R. Gettu, A. Patel, V. Rathi, S. Prakasan, A. Basavaraj, S. Palaniappan, S. Maity, Influence of supplementary cementitious materials on the sustainability parameters of cements and concretes in the Indian context, Materials and Structures, 52 (2019) 10.

[2] C. Poon, L. Lam, Y. Wong, A study on high strength concrete prepared with large volumes of low calcium fly ash, Cement and Concrete Research, 30 (2000) 447-455.

[3] K. Ampadu, K. Torii, M. Kawamura, Beneficial effect of fly ash on chloride diffusivity of hardened cement paste, Cement and Concrete Research, 29 (1999) 585-590.

[4] L. Lam, Y. Wong, C. Poon, Degree of hydration and gel/space ratio of high-volume fly ash/cement systems, Cement and Concrete Research, 30 (2000) 747-756.

[5] J. Yajun, J. Cahyadi, Simulation of silica fume blended cement hydration, Materials and Structures, 37 (2004) 397-404.

[6] W. Wilson, J. Rivera-Torres, L. Sorelli, A. Durán-Herrera, A. Tagnit-Hamou, The micromechanical signature of high-volume natural pozzolan concrete by combined statistical nanoindentation and SEM-EDS analyses, Cement and Concrete Research, 91 (2017) 1-12.

[7] D.P. Bentz, O.M. Jensen, A. Coats, F.P. Glasser, Influence of silica fume on diffusivity in cement-based materials: I. Experimental and computer modeling studies on cement pastes, Cement and Concrete Research, 30 (2000) 953-962.

[8] Y. Maltais, J. Marchand, Influence of curing temperature on cement hydration and mechanical strength development of fly ash mortars, Cement and Concrete Research, 27 (1997) 1009-1020.

[9] S. Zhuang, Q. Wang, Y. Zhu, Research on the resistance to saline soil erosion of high-volume mineral admixture steam-cured concrete, Construction and Building Materials, 202 (2019) 1-10.

[10] A. Korpa, R. Trettin, Very high early strength of ultra-high performance concrete containing nanoscale pozzolans using the microwave heat curing method, Advances in Cement Research, 20 (2008) 175-184.

[11] M. Narmluk, T. Nawa, Effect of fly ash on the kinetics of Portland cement hydration at different curing temperatures, Cement and Concrete Research, 41 (2011) 579-589.

[12] J. Escalante-Garcıa, J. Sharp, Effect of temperature on the hydration of the main clinker phases in Portland cements: Part II, blended cements, Cement and Concrete Research, 28 (1998) 1259-1274.

[13] K. De Weerdt, M.B. Haha, G. Le Saout, K. Kjellsen, H. Justnes, B. Lothenbach, The effect of temperature on the hydration of composite cements containing limestone powder and fly ash, Materials and Structures, 45 (2012) 1101-1114.

[14] P.T. Durdziński, M.B. Haha, S.A. Bernal, N. De Belie, E. Gruyaert, B. Lothenbach, E.M. Méndez, J.L. Provis, A. Schöler, C. Stabler, Outcomes of the RILEM round robin on degree of

reaction of slag and fly ash in blended cements, Materials and Structures, 50 (2017) 135.
[15] X.-Y. Wang, H.-S. Lee, Modeling the hydration of concrete incorporating fly ash or slag, Cement and concrete Research, 40 (2010) 984-996.
[16] K.-B. Park, T. Noguchi, J. Plawsky, Modeling of hydration reactions using neural networks to predict the average properties of cement paste, Cement and Concrete Research, 35 (2005) 1676-1684.
[17] T. Wang, T. Ishida, Multiphase pozzolanic reaction model of low-calcium fly ash in cement systems, Cement and Concrete Research, 122 (2019) 274-287.
[18] K. Maekawa, R. Chaube, T. Kishi, Modelling of concrete performance, 1999.
[19] P. Gao, Simulation of hydration and microstructure development of blended cements, PhD thesis, Delft University of Technology, 2018.
[20] G. Ye, K. Van Breugel, A. Fraaij, Three-dimensional microstructure analysis of numerically simulated cementitious materials, Cement and Concrete Research, 33 (2003) 215-222.
[21] S. Bishnoi, S. Joseph, A. Kaur, Microstructural modelling of the strength of mortars containing fly ash using µic, Construction and Building Materials, 163 (2018) 912-920.
[22] S. Bishnoi, K.L. Scrivener, µic: A new platform for modelling the hydration of cements, Cement and Concrete Research, 39 (2009) 266-274.
[23] C. Liu, F. Wang, M. Zhang, Modelling of 3D microstructure and effective diffusivity of fly ash blended cement paste, Cement and Concrete Composites, (2020) 103586.
[24] D.P. Bentz, S. Remond, Incorporation of fly ash into a 3-D cement hydration microstructure model, US Department of Commerce, Technology Administration, National Institute of Standards and Technology, 1997.
[25] C. Liu, D. Xie, W. She, Z. Liu, G. Liu, L. Yang, Y. Zhang, Numerical modelling of elastic modulus and diffusion coefficient of concrete as a three-phase composite material, Construction and Building Materials, 189 (2018) 1251-1263.
[26] J. Cabrera, T. Dodd, S. Nwaubani, Effect of Curing Temperature on the Chloride Ion Diffusion of Superplasticized Cement and Fly Ash pastes, Special Publication, 139 (1993) 61-76.
[27] S.D. Abyaneh, H. Wong, N. Buenfeld, Modelling the diffusivity of mortar and concrete using a three-dimensional mesostructure with several aggregate shapes, Computational Materials Science, 78 (2013) 63-73.
[28] J.J. Thomas, J.J. Biernacki, J.W. Bullard, S. Bishnoi, J.S. Dolado, G.W. Scherer, A. Luttge, Modeling and simulation of cement hydration kinetics and microstructure development, Cement and Concrete Research, 41 (2011) 1257-1278.
[29] G. Ye, K. Van Breugel, A. Fraaij, Experimental study and numerical simulation on the formation of microstructure in cementitious materials at early age, Cement and Concrete Research, 33 (2003) 233-239.

[30] D.P. Bentz, D.P. CEMHYD3D: A three-dimensional cement hydration and microstructure development modelling package. Version 3.0, US Department of Commerce, National Institute of Standards and Technology, 2005.
[31] R.T. Chancey, P. Stutzman, M.C. Juenger, D.W. Fowler, Comprehensive phase characterization of crystalline and amorphous phases of a Class F fly ash, Cement and Concrete Research, 40 (2010) 146-156.
[32] P.T. Durdziński, C.F. Dunant, M.B. Haha, K.L. Scrivener, A new quantification method based on SEM-EDS to assess fly ash composition and study the reaction of its individual components in hydrating cement paste, Cement and Concrete Research, 73 (2015) 111-122.
[33] N. Robeyst, C.U. Grosse, N. De Belie, Relating ultrasonic measurements on fresh concrete with mineral additions to the microstructure development simulated by Cemhyd3D, Cement and Concrete Composites, 33 (2011) 680-693.
[34] T.C. Powers, Structure and physical properties of hardened Portland cement paste, Journal of the American Ceramic Society, 41 (1958) 1-6.
[35] H.M. Jennings, A model for the microstructure of calcium silicate hydrate in cement paste, Cement and Concrete Research, 30 (2000) 101-116.
[36] H.M. Jennings, Colloid model of C-S-H and implications to the problem of creep and shrinkage, Materials and Structures, 37 (2004) 59-70.
[37] S. Hanehara, F. Tomosawa, M. Kobayakawa, K. Hwang, Effects of water/powder ratio, mixing ratio of fly ash, and curing temperature on pozzolanic reaction of fly ash in cement paste, Cement and Concrete Research, 31 (2001) 31-39.
[38] E. Sakai, S. Miyahara, S. Ohsawa, S.-H. Lee, M. Daimon, Hydration of fly ash cement, Cement and Concrete Research, 35 (2005) 1135-1140.
[39] J. Escalante-Garcıa, J. Sharp, The microstructure and mechanical properties of blended cements hydrated at various temperatures, Cement and Concrete Research, 31 (2001) 695-702.
[40] Q. Zeng, K. Li, T. Fen-Chong, P. Dangla, Pore structure characterization of cement pastes blended with high-volume fly-ash, Cement and Concrete Research, 42 (2012) 194-204.
[41] F. Han, J. Liu, P. Yan, Comparative study of reaction degree of mineral admixture by selective dissolution and image analysis, Construction and Building Materials, 114 (2016) 946-955.
[42] T. Wang, Modeling of Pozzolanic reaction of siliceous fly ash in cement system based on its material characterization, PhD thesis, The University of Tokyo, 2017.
[43] A. Fernández-Jiménez, A. Palomo, Characterisation of fly ashes. Potential reactivity as alkaline cements, Fuel, 82 (2003) 2259-2265.
[44] M. Sofi, E. Lumantarna, Z. Zhou, R. San Nicolas, P. Mendis, From hydration to strength properties of fly ash based mortar, Journal of Materials Science and Chemical Engineering, 5 (2017)

63.
[45] P.T. Durdziński, M. Ben Haha, S.A. Bernal, N. De Belie, E. Gruyaert, B. Lothenbach, E. Menéndez Méndez, J.L. Provis, A. Schöler, C. Stabler, Z. Tan, Y. Villagrán Zaccardi, A. Vollpracht, F. Winnefeld, M. Zając, K.L. Scrivener, Outcomes of the RILEM round robin on degree of reaction of slag and fly ash in blended cements, Materials and Structures, 50 (2017).
[46] C. Liu, G. Liu, Z. Liu, L. Yang, M. Zhang, Y. Zhang, Numerical simulation of the effect of cement particle shapes on capillary pore structures in hardened cement pastes, Construction and Building Materials, 173 (2018) 615-628.
[47] J.M. Hovadik, D.K. Larue, Static characterizations of reservoirs: refining the concepts of connectivity and continuity, Petroleum Geoscience, 13 (2007) 195-211.
[48] C. Liu, Z. Liu, Y. Zhang, A multi-scale framework for modelling effective gas diffusivity in dry cement paste: Combined effects of surface, Knudsen and molecular diffusion, Cement and Concrete Research, 131 (2020) 106035.
[49] R.A. Robinson, Stokes, RH electrolyte solutions, London, Butterworths Scientific Publications, 19550 (1959) 540-544.
[50] H. Ma, D. Hou, Z. Li, Two-scale modeling of transport properties of cement paste: Formation factor, electrical conductivity and chloride diffusivity, Computational Materials Science, 110 (2015) 270-280.
[51] P. Pivonka, C. Hellmich, D. Smith, Microscopic effects on chloride diffusivity of cement pastes—a scale-transition analysis, Cement and Concrete Research, 34 (2004) 2251-2260.
[52] Y. Zhang, C. Liu, Z. Liu, G. Liu, L. Yang, Modelling of diffusion behavior of ions in low-density and high-density calcium silicate hydrate, Construction and Building Materials, 155 (2017) 965-980.
[53] A. Ramezanianpour, V. Malhotra, Effect of curing on the compressive strength, resistance to chloride-ion penetration and porosity of concretes incorporating slag, fly ash or silica fume, Cement and Concrete Romposites, 17 (1995) 125-133.
[54] R.A. Patel, J. Perko, D. Jacques, G. De Schutter, G. Ye, K. Van Bruegel, Effective diffusivity of cement pastes from virtual microstructures: Role of gel porosity and capillary pore percolation, Construction and Building Materials, 165 (2018) 833-845.
[55] P. Li, D. Su, S. Wang, Z. Fan, Influence of binder composition and concrete pore structure on chloride diffusion coefficient in concrete, Journal of Wuhan University of Technology-Mater. Sci. Ed., 26 (2011) 160-164.
[56] Q. Zhou, F.P. Glasser, Thermal stability and decomposition mechanisms of ettringite at< 120 °C, Cement and Concrete Research, 31 (2001) 1333-1339.
[57] F. Deschner, B. Lothenbach, F. Winnefeld, J. Neubauer, Effect of temperature on the hydration of Portland cement blended with siliceous fly ash, Cement and Concrete Research, 52 (2013) 169-

181.
[58] D. Hou, T. Li, P. Wang, Molecular dynamics study on the structure and dynamics of NaCl solution transport in the nanometer channel of CASH gel, ACS Sustainable Chemistry & Engineering, 6 (2018) 9498-9509.

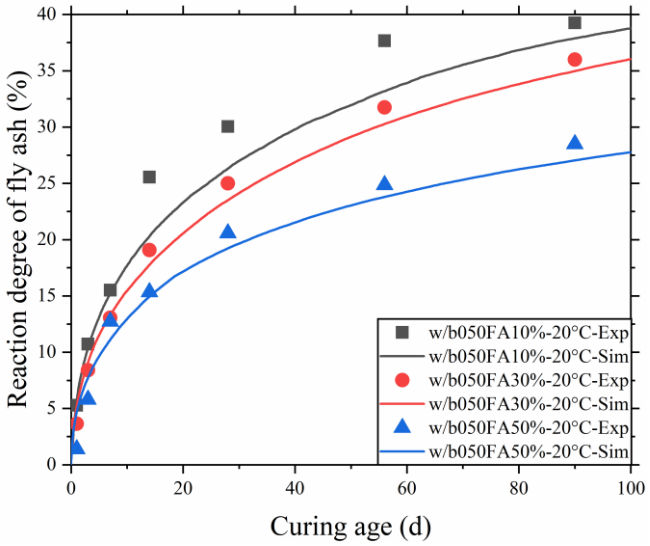

Fig. 1. Reaction degree of fly ash in blended cement pastes with w/b = 0.50 and various fly ash contents at 20 °C as a function of curing age in this study.

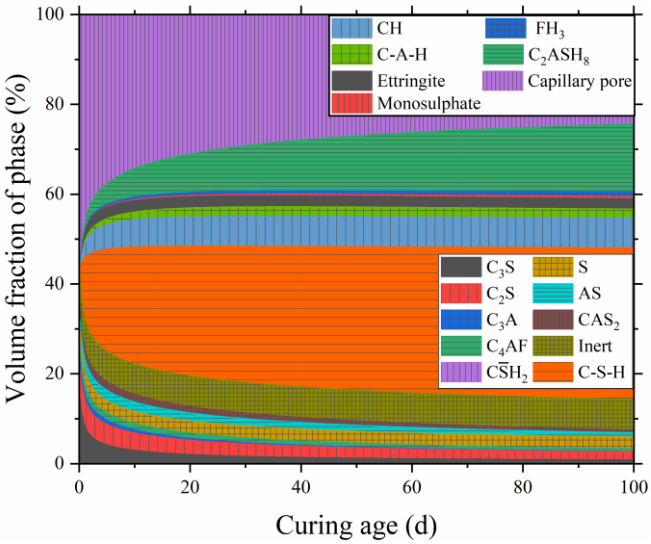

Fig. 2. Simulated volume fractions of solid phases and capillary pore in fly ash blended cement paste with w/b = 0.50 and fly ash content of 30% at 20 °C as a function of curing age.

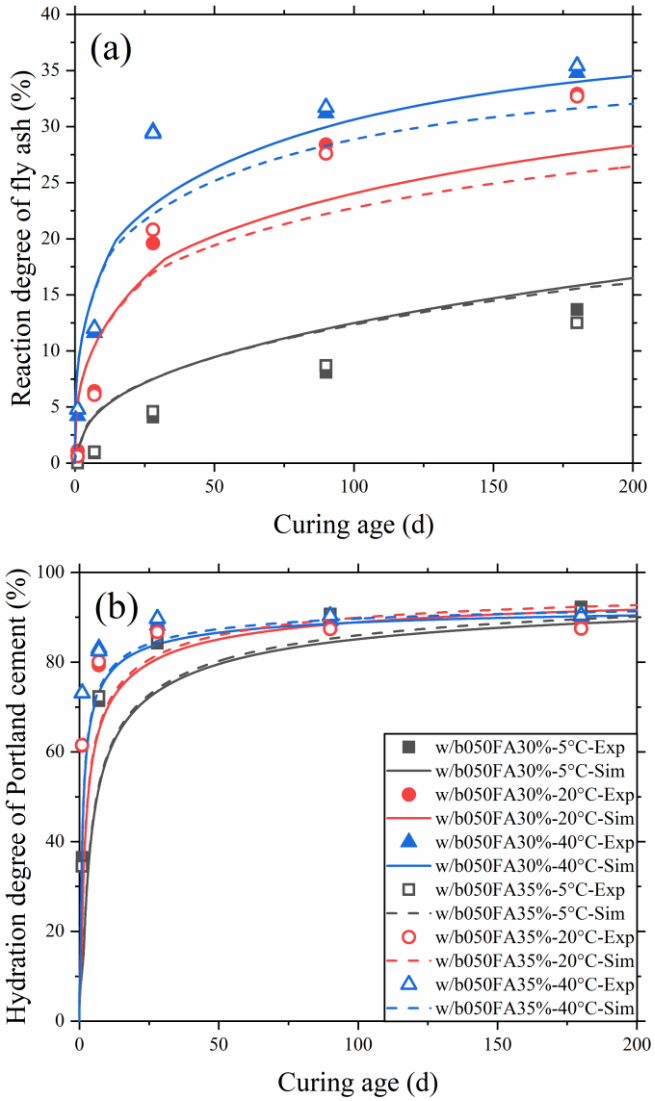

Fig. 3. Reaction degree of fly ash (a) and hydration degree of Portland cement (b) in blended cement pastes with w/b = 0.50 and fly ash contents of 30% and 35% at 5 °C, 20 °C and 40 °C as a function of curing age after Weerdt et al. [13].

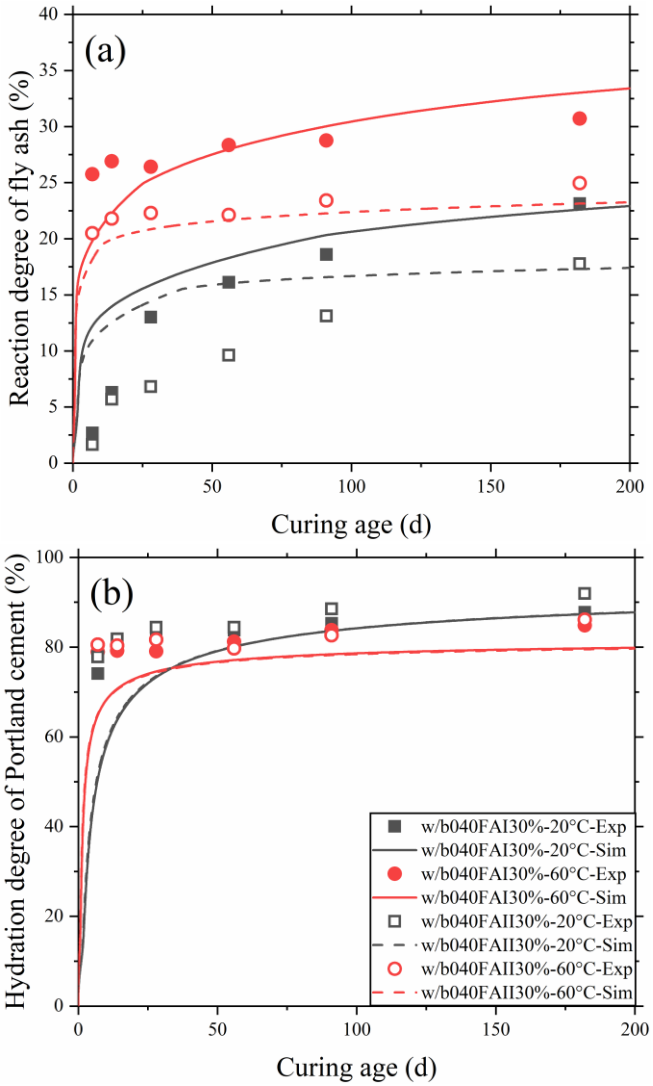

Fig. 4. Reaction degree of fly ash (a) and hydration degree of Portland cement (b) in blended cement pastes with w/b = 0.40 and fly ash content of 30% at 20 °C and 60 °C as a function of curing age after Wang and Ishida [17, 42].

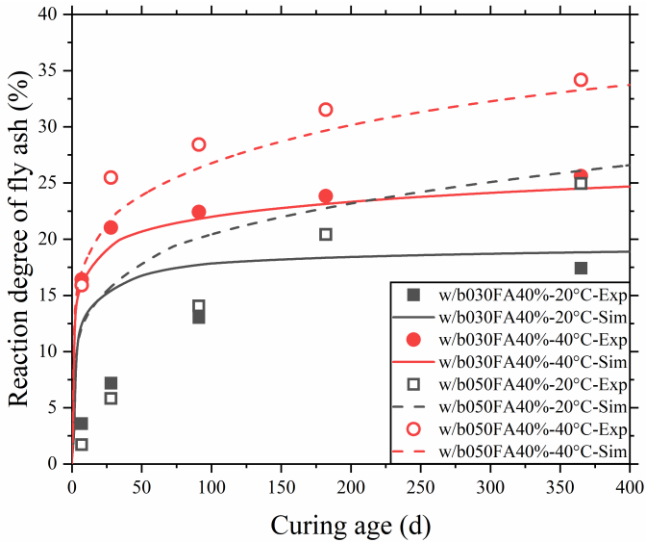

Fig. 5. Reaction degree of fly ash in blended cement pastes with w/b = 0.30 and 0.50 and fly ash content of 40% at 20 °C and 40 °C as a function of curing age after Hanehara et al. [37].

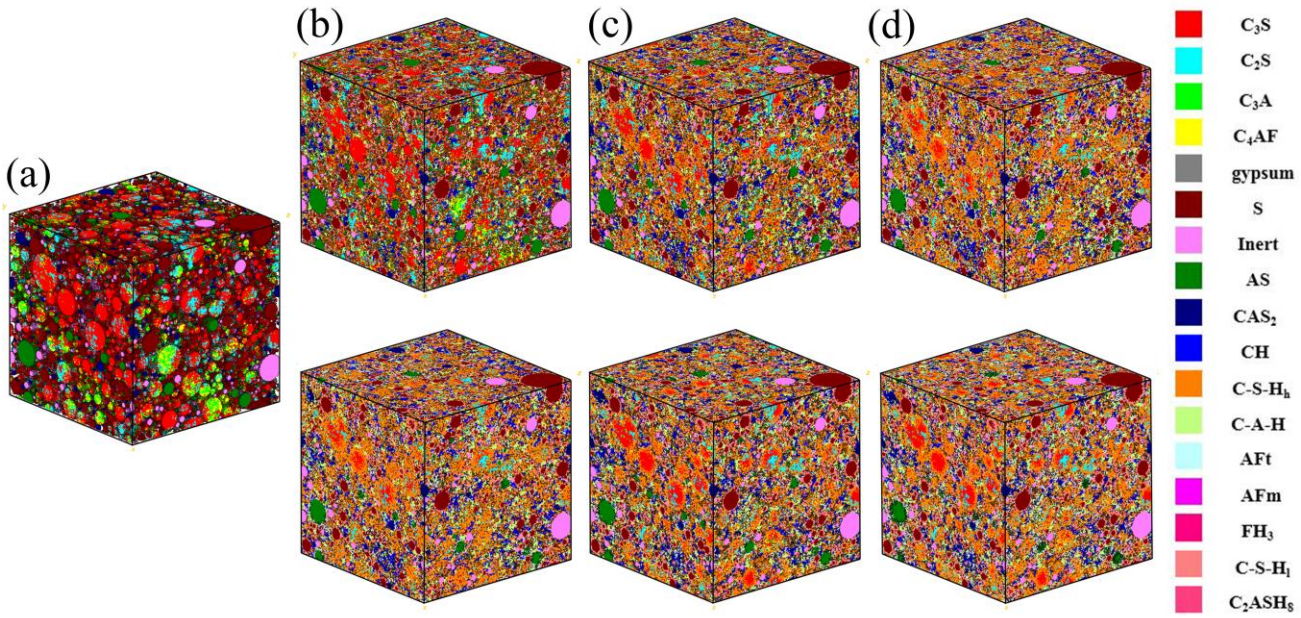

Fig. 6. Evolution of solid phases in microstructure of fly ash blended cement pastes with w/b = 0.40 and fly ash (FA I) content of 30% at (a) 0 d, (b) 3 d, (c) 28 d, and (d) 180 d (top row – 20 °C, bottom row – 60 °C).

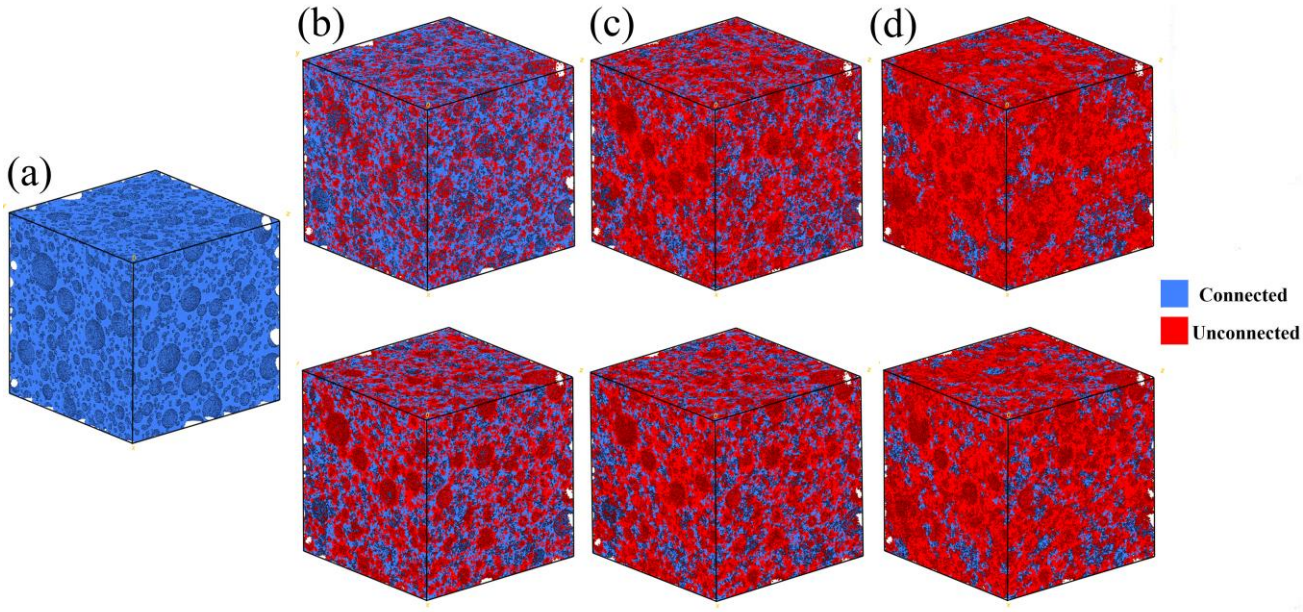

Fig. 7. Evolution of capillary pore structure of fly ash blended cement paste with w/b = 0.40 and fly ash (FA I) content of 30% at (a) 0 d, (b) 3 d, (c) 28 d, and (d) 180 d (top row – 20 °C, bottom row – 60 °C).

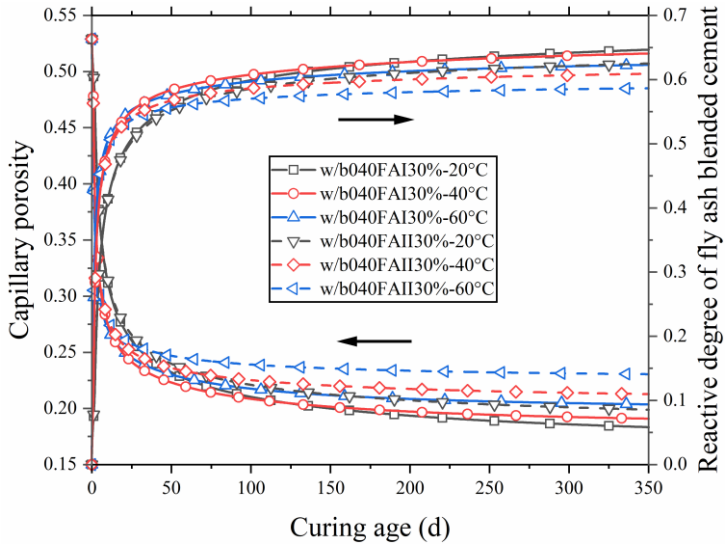

Fig. 8. Capillary porosity and reactive degree of fly ash blended cement in paste with w/b = 0.40 and fly ash content of 30% at 20 °C, 40 °C and 60 °C as a function of curing age.

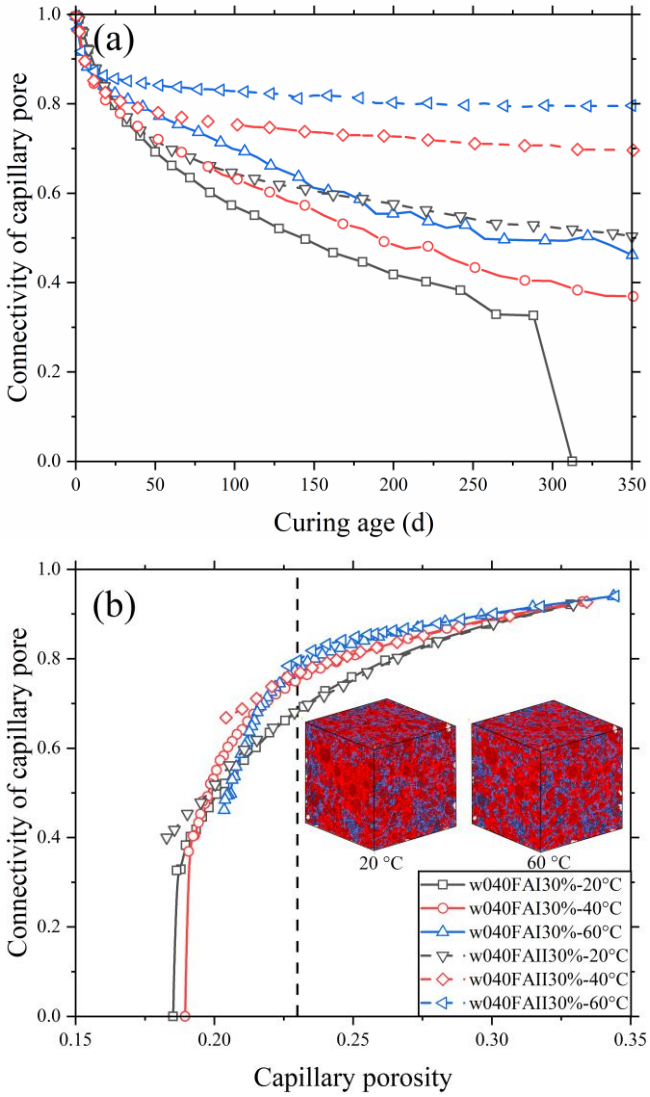

Fig. 9. Connectivity of capillary pore in fly ash blended cement paste with w/b = 0.40 and fly ash content of 30% at 20 °C, 40°C and 60 °C as a function of curing age (a) and capillary porosity (b).

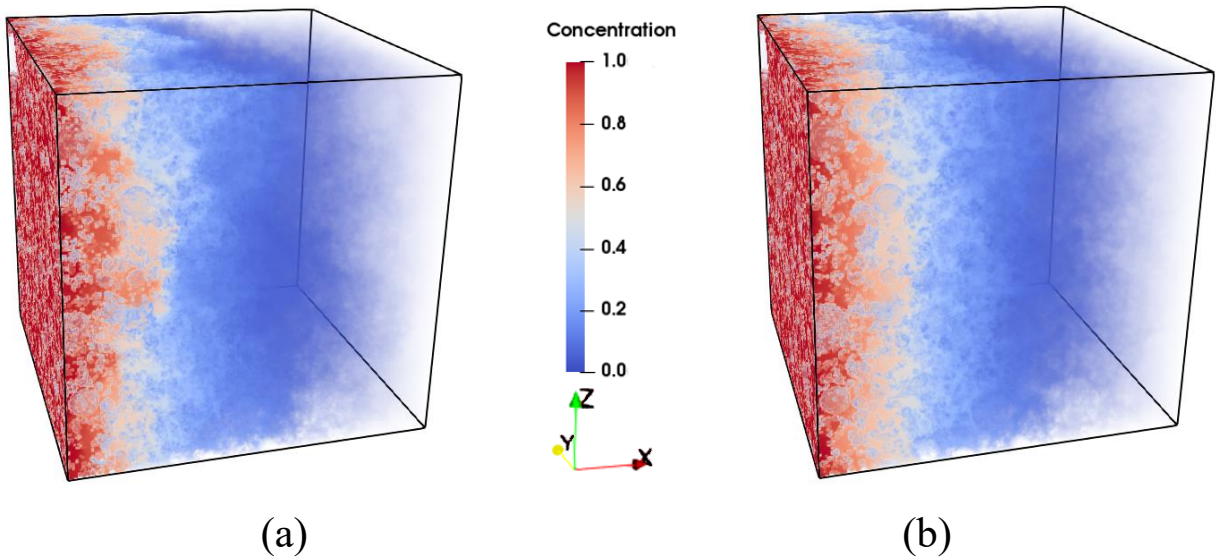

Fig. 10. Steady-state ionic concentration distribution in blended cement paste with w/b = 0.40 and fly ash (FA I) content of 30% cured at 20 °C (a) and 60 °C (b) for 28 d.

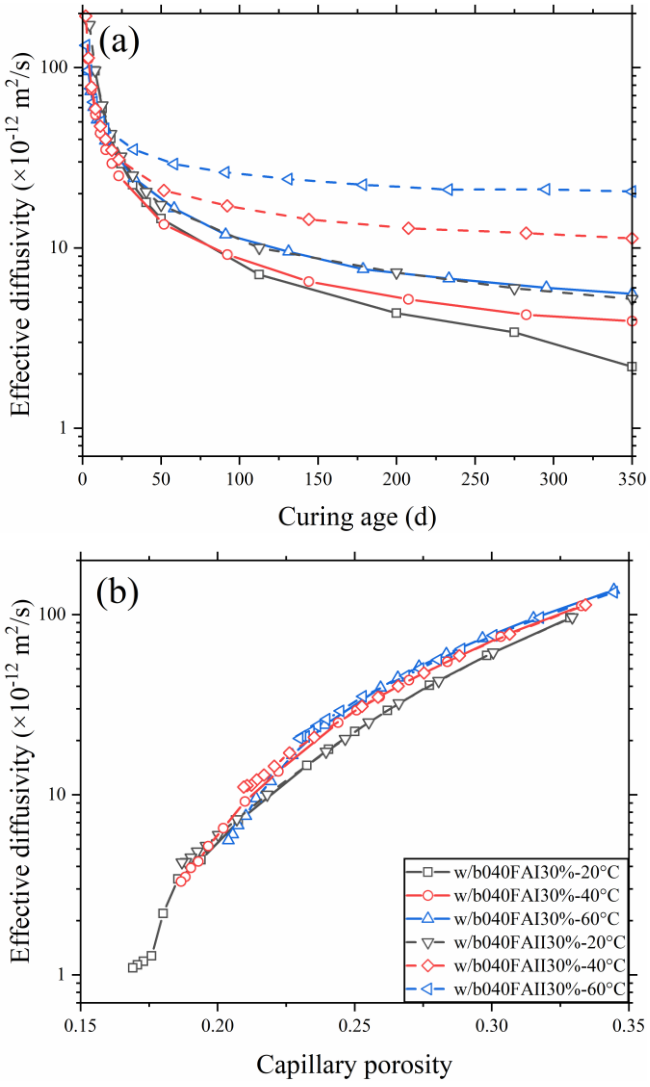

Fig. 11. Ionic diffusivity of fly ash blended cement paste with w/b = 0.40 and fly ash content of 30% at 20 °C, 40 °C and 60 °C as a function of curing age (a) and capillary porosity (b).

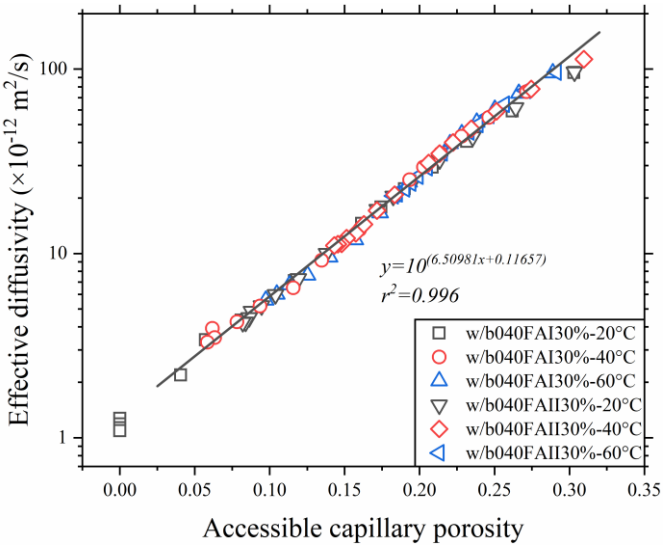

Fig. 12. Ionic diffusivity of fly ash blended cement paste with w/b = 0.40 and fly ash content of 30% at 20 °C, 40 °C and 60 °C as a function of accessible capillary porosity.

Table 1. Chemical composition and physical properties of Portland cement and fly ash.

Chemical composition /physical properties	This study		Weerdt et al. [13]		Wang and Ishida [17]			Hanehara et al. [37]	
	PC	FA	PC	FA	PC	FA I	FA II	PC	FA
SiO_2 (%)	-	47.86	-	50.00	-	64.10	63.78	-	54.40
Al_2O_3 (%)	-	32.50	-	23.90	-	20.23	19.78	-	31.1
CaO (%)	-	4.09	-	6.32	-	2.19	4.65	-	4.50
MgO (%)	-	1.05	-	2.12	-	0.70	0.69	-	0.80
Na_2O (%)	-	0.55	-	0.63	-	0.58	0.54	-	0.60
K_2O (%)	-	1.62	-	1.42	-	1.24	1.07	-	0.80
Fe_2O_3 (%)	-	4.52	-	6.03	-	4.17	4.12	-	4.60
C_3S (%)	56.00	-	58.70	-	65.50	-	-	-	-
C_2S (%)	25.66	-	20.65	-	15.90	-	-	-	-
C_3A (%)	7.49	-	11.95	-	8.07	-	-	-	-
C_4AF (%)	10.85	-	8.70	-	8.77	-	-	-	-
Mullite ($Al_6Si_2O_{13}$, %)	-	11.77	-	18.30	-	10.92	14.18	-	-
Quartz (SiO_2, %)	-	23.64	-	12.30	-	7.21	10.28	-	-
Amorphous (%)	-	64.59	-	69.40	-	81.15	74.09	-	-
Fineness (m^2/kg)	369	454	450	450	335	394	407	337	400
Density (g/cm^3)	3.15	2.24	3.15	2.49	3.15	2.28	2.34	3.14	2.33

Table 2. Volume fractions of mineral phases of fly ash used in the simulation.

Mineral phase (vol%)	This study	Weerdt et al. [13]	Wang and Ishida [17]	
			FA I	FA II
CAS_2	19.30	36.06	11.20	23.38
AS	20.90	1.43	12.71	2.22
S	22.40	30.09	58.76	49.93
Inert	37.40	32.42	17.33	24.47